Cross-Flow of Flux Lines in the Weak Link Regime of High-T_c Superconductors

M. A. R. LeBlanc,[1] Selahattin Celebi,[2] Sean X. Wang,[1] and Vladimir Plechácêk[3]

[1]*Physics Department, University of Ottawa, Ottawa, Canada K1N 6N5*

[2]*Physics Department, Karadeniz Technical University, Trabzon, Turkey 61080*

[3]*Institute of Physics, Czechoslovak Academy of Sciences, Cukrovarnická 10, 16200 Prague 6, Czechoslovakian Republic*

(Received 30 March 1993)

The evolution of the magnetic flux density in the cavity and wall of tubes of high-T_c superconductors subjected to an azimuthal field in the presence of axial fields provides dramatic evidence of cutting and cross-flow of the flux lines in the weak link regime.

PACS numbers: 74.60.Ec, 74.60.Ge, 74.60.Jg

The possibility that nonparallel flux vortices in classical and high-T_c superconductors can disentangle and traverse each other via cutting and interconnection processes continues to be a subject of controversy [1–9] because of the large condensation energy barrier opposing such a process, although various experiments supporting such phenomena have already been published [10–15]. Recently LeBlanc *et al.* [15] reported on an experiment which provides new evidence that helical flux lines migrate through each other in the wall of hollow cylinders of conventional type-II superconductors as an ambient helical magnetic field is slowly swept in magnitude between H_{c1} and H_{c2} while its pitch is simultaneously made to vary. In this Letter we present observations on hollow cylinders of oxide high-T_c superconductors at 77 K which carry the clear signature of cutting and cross-flow of flux lines in the weak link regime of these granular ceramic materials. The experimental arrangement is similar to that exploited by LeBlanc *et al.* [15]. We have, however, introduced an important new feature which provides additional information on the traffic of the flux lines. In our work the "sample tube" is embraced concentrically by a second high-T_c tube of the same material. The setup is sketched in Fig. 1 and described below.

The message that flux-line cutting and cross-flow of interpenetrating vortex arrays take place emerges from consideration of concurrent phenomena displayed in Fig. 2 and which we now outline.

To set the stage for these events the tubes are first field cooled in a homogeneous magnetic field, $H_{\parallel}$, provided by a long solenoid and directed along the axis of the tubes. The applied magnetic field, $H_{\parallel}$, is maintained stationary at the selected value throughout the history of each measurement. A small fraction of the axial magnetic flux initially permeating the wall of the inner tube in the normal state is expelled from the wall during the field cooling procedure into the cavity of the inner tube causing $\langle B_z\rangle_{\text{hole}}$, the axial magnetic flux density in that finite closed "reservoir," to rise slightly. The outer tube is cooled after the inner tube, hence $\langle B_z\rangle_{\text{annular}}$, the axial magnetic flux density, in the annular volume between the two nesting tubes (denoted reservoir 2), rises slightly during the field cooling procedure due to radial inward expulsion of axial magnetic flux from the wall of the outer tube. We now turn to the fascinating behavior which is the crux of our narrative (see Fig. 2).

An azimuthal magnetic field, H_ϕ, provided by a toroidal magnet coil, uniformly embracing the entire wall of the inner tube, is now slowly impressed. The following set of events are witnessed to occur in unison as the total ambient magnetic field, $\mathbf{H}_t = \hat{\boldsymbol{\phi}} H_\phi + \hat{\mathbf{z}} B_z/\mu_0$ along the surfaces of the inner tube is caused to increase in magnitude while simultaneously changing its direction from purely axial to helical.

(i) $\langle B_\phi\rangle_{\text{wall}}$, the spatial average of the azimuthal flux density threading the wall of the inner tube, is seen to grow monotonically from zero [see Fig. 2(a)]. (ii) $\langle B_z\rangle_{\text{wall}}$, the spatial average of the axial flux density permeating the wall of the inner tube, is observed to diminish and trace a valley [see Fig. 2(c)]. The fate of the axial flux disappearing from the wall is elucidated by the fol-

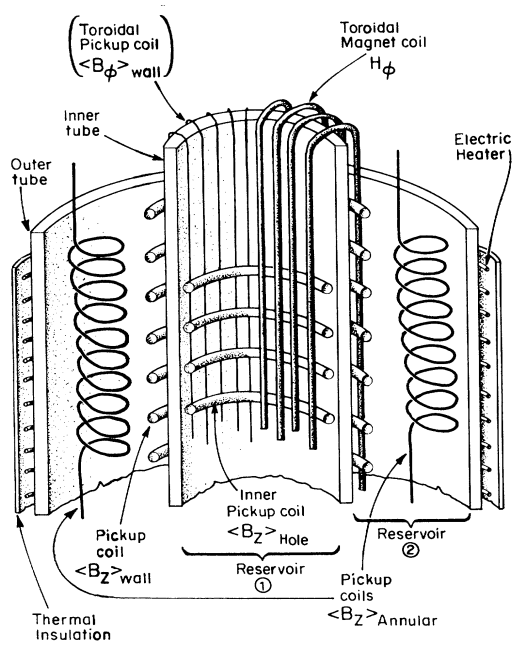

FIG. 1. Schematic of the sample arrangement. The electric heater embracing the inner tube is not shown.

0031-9007/93/71(20)/3367(4)$06.00

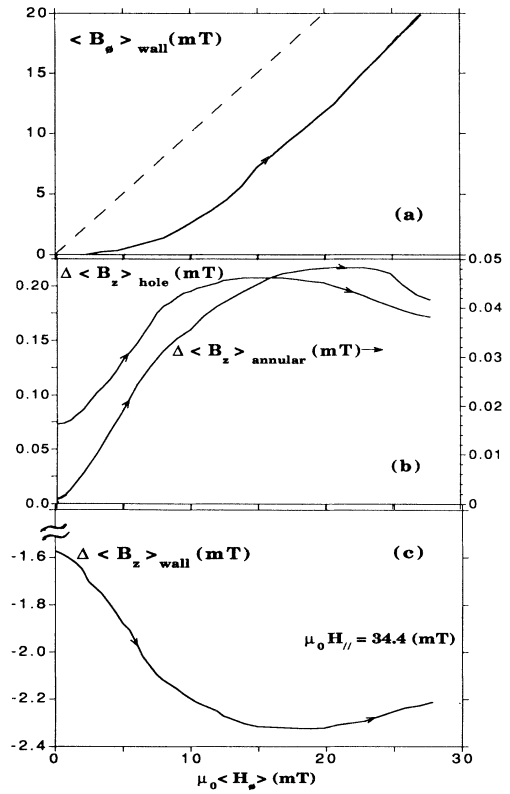

FIG. 2. Four events occurring simultaneously as the azimuthal field $\langle H_\phi \rangle$ is impressed. (a) The rise of $\langle B_\phi \rangle_{\text{wall}}$, the azimuthal flux density in the wall (solid line). (b) The evolution of the axial flux density in the hole ($\langle B_z \rangle_{\text{hole}}$) and the annular reservoir ($\langle B_z \rangle_{\text{annular}}$). (c) The evolution of $\langle B_z \rangle_{\text{wall}}$, the axial flux density permeating the wall. The specimen field cooled in an externally applied axial field $\mu_0 H_\parallel = 344$ G which was maintained fixed as H_ϕ was impressed. The outer tube cooled after the inner tube, hence, $\langle B_z \rangle_{\text{annular}} \approx \mu_0 H_\parallel$ before $\langle H_\phi \rangle$ is applied. $T = 77$ K.

lowing observations. (iii) $\langle B_z \rangle_{\text{hole}}$, the axial magnetic flux density threading reservoir 1 (the hole), is seen to rise and traverse a peak [see Fig. 2(b)]. (iv) $\langle B_z \rangle_{\text{annular}}$, the axial magnetic flux density threading reservoir 2, is also seen to rise in approximate phase with $\langle B_z \rangle_{\text{hole}}$ and trace a summit [see Fig. 2(b)].

The first of these four observations is consistent with the universally accepted view that an increase in magnitude of a magnetic field, $|\mathbf{H}| > H_{c1}$, along the surfaces of a type-II superconductor, causes flux lines to nucleate at the surfaces, enter, and penetrate into the bulk of the material. The three other observations unambiguously testify that, concurrently, magnetic flux is migrating from the wall of the inner tube and is released into the two reservoirs adjacent to the wall. Indeed, the total increment of axial flux appearing in the two reservoirs corresponds closely to the depletion of axial flux from the wall of the inner tube.

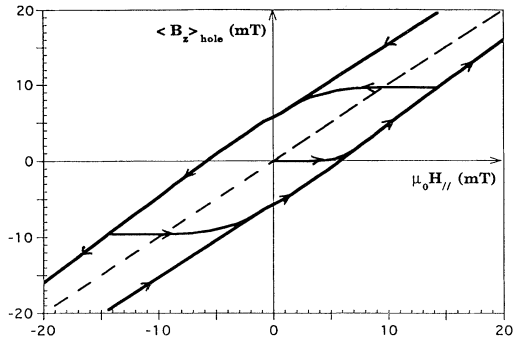

FIG. 3. Evolution of the axial flux density in the cavity of the (isolated) inner tube as $H_\parallel$ is applied to a "virgin" tube then reduced to zero after a sweep to a large value (upper curve), or an intermediate value (middle solid curve). Bottom curve is observed after a sweep to a large negative value. $T = 77$ K.

The phenomena we report have been observed at 77 K in tubes of the two polycrystalline materials we have investigated; 2223 phase $(Bi_{0.9}Pb_{0.1})_2Sr_2Ca_2Cu_3O_{10}$ and $YBa_2Cu_3O_{7-x}$. The pertinent data for the two materials are qualitatively identical. We present results for the former sample since it exhibits an intergranular critical current density $\langle j_c \rangle$ an order of magnitude greater than the latter in the field range under scrutiny. The evolution of $\langle B_z \rangle_{\text{hole}}$ vs $\mu_0 H_\parallel$ for the isolated inner tube is displayed in Fig. 3. The response of the outer tube is identical. The capacity of the tubes to oppose entry or exit of axial flux is diminished when a static H_ϕ is present. This indicates that flux line cutting depresses the circumferential critical current. The inner (outer) tube has an inner diameter of 1.4 cm (3.07 cm) and outer diameter of 1.72 cm (3.484 cm) and a length of 3.7 cm (2.84 cm).

The evolution of $\langle B_z \rangle_{\text{hole}}$, $\langle B_z \rangle_{\text{annular}}$, $\langle B_z \rangle_{\text{wall}}$, and $\langle B_\phi \rangle_{\text{wall}}$ is continuously monitored using four pickup coils which separately feed amplifier integrators which drive the Y axes of XY recorders. For Fig. 2 (Fig. 3) the X axes are driven by a signal proportional to H_ϕ ($H_\parallel$) provided by a series shunt in the circuit of the toroidal magnet coil generating H_ϕ (solenoid generating $H_\parallel$). The pickup coils are calibrated by comparing the responses to weak H_ϕ or $H_\parallel$ with the tubes at 77 K and just above T_c. The temperature of the tubes is raised from 77 K to T_c using noninductive manganin wire heaters uniformly and directly embracing the entire external surface of the two concentric tubes.

The "nesting" of the four pickup coils and the toroidal magnet coil is indicated schematically in Fig. 1. The inner pickup coil monitoring $\langle B_z \rangle_{\text{hole}}$ extends along the central half of the length of the inner tube. $\langle B_z \rangle_{\text{annular}}$ is monitored by five series connected pickup coils optimally occupying the available annular space. The toroidal pickup coil, uniformly surrounding the circumference of the wall, monitors $\langle B_\phi \rangle_{\text{wall}}$ and is embraced by the toroidal magnet coil generating H_ϕ. The determination of $\langle B_z \rangle_{\text{wall}}$

is a composite measurement obtained as follows. A pickup coil embraces the waist of the inner tube and records $\Delta\phi_{z\,\mathrm{total}}$, the change in the total axial magnetic flux threading it. Since, $\phi_{z\,\mathrm{total}}=\langle B_z\rangle_{\mathrm{total}}\pi R_0^2=\phi_{z\,\mathrm{hole}}+\phi_{z\,\mathrm{wall}}=\langle B_z\rangle_{\mathrm{hole}}\pi R_i^2+\langle B_z\rangle_{\mathrm{wall}}\pi(R_0^2-R_i^2)$ (where R_i and R_0 are the inner and outer radius of the inner tube), we can determine $\langle B_z\rangle_{\mathrm{wall}}$ by subtracting the signal from the inner pickup coil, which detects $\Delta\phi_{z\,\mathrm{hole}}$, from that of the outer pickup coil, either electronically or digitally.

The toroidal magnet coil generating H_ϕ comprises 48 turns of copper wire. We ensure that this coil generates no axial field. From Ampere's law, $\oint\mathbf{H}\cdot d\boldsymbol{l}=nI$, the azimuthal field applied to the wall of the inner tube reads $H_\phi=nI/2\pi r$, and its spatial average reads $\langle H_\phi\rangle=[nI/2\pi(R_0-R_i)]\ln(0/R_i)$ (where n is the number of turns and I is the current flowing in each turn). We emphasize that the outer tube experiences no azimuthal field since by Ampere's law, $H_\phi=0$ outside the toroidal magnet coil.

Various aspects of the phenomenon of cutting and cross-flow of flux lines have been examined theoretically by several workers [1,2,16–22]. The phenomenological framework developed by Clem and Perez-Gonzalez [18, 19,21] is now applied to describe the evolution of $\langle B_z\rangle_{\mathrm{wall}}$ vs H_ϕ increasing in stationary $H_\parallel$.

For computational ease we use planar geometry since the wall thickness, $R_0-R_i=2X$, is small compared to the radius of the tube. The tube is viewed as infinitely long along the z axis. The unit vector $\hat{\mathbf{y}}$ replaces the azimuthal unit vector $\hat{\boldsymbol{\phi}}$. The x axis lies along the radius of the tube and $(R_i+R_0)/2$, the midplane of the wall, is situated at $x=0$. We take the azimuthal magnetic fields along the surfaces of the wall, $H_\phi(R_i)=\langle H_\phi\rangle=H(R_0)$ and hence ignore the small variation of $H_\phi(r)$ over the wall thickness. Also we let $\langle B_z\rangle_{\mathrm{hole}}=\mu_0H_\parallel=\langle B_z\rangle_{\mathrm{annular}}$, and hence neglect the increments of the axial fields in the reservoirs as H_ϕ is increased. Thus the $\mathbf{B}(x)$ profiles are regarded as symmetric with respect to the "midplane" (midradius) $x=0$. We take $\mathbf{B}(x)=\hat{\mathbf{z}}\mu_0H_\parallel$ before H_ϕ is applied and hence ignore the small variation in the B profile accompanying the flux expulsion (Meissner effect) during the field cooling. Intrinsic reversible diamagnetism is not taken into account, hence we let $\mathbf{B}(x)=\mu_0\mathbf{H}(x)$.

Within the context of the Clem and Perez-Gonzalez model we stipulate that cutting-transport (CT), transport (T), cutting (C), and "inert" (0) zones arise as the configurations of magnetic flux density, $\mathbf{B}(x)=\hat{\mathbf{y}}B_y(x)+\hat{\mathbf{z}}B_z(x)$, evolve through sequences of critical states as H_ϕ is impressed with $H_\parallel$ held fixed. A flux line cutting (C) zone vanishes when the disturbances in $|\mathbf{B}(x)|$ and $\alpha(x)=\tan^{-1}[B_y(x)/B_z(x)]$ have penetrated to the midplane.

The equations of the Clem–Perez-Gonzalez theory for CT zones then read

$$\mu_0 j_{c\perp}=\pm\frac{dB}{dx},\quad \mu_0 j_{c\parallel}=\pm B\frac{d\alpha}{dx}, \tag{1}$$

where $j_{c\perp}$ and $j_{c\parallel}$ are the critical current densities for flux line depinning and flux line cutting flowing perpendicular and parallel to $\mathbf{B}(x)$. The wall is viewed as isotropic and homogeneous. The calculation focuses on the intergrain critical current densities $j_{c\perp}$ and $j_{c\parallel}$ [and associated $\mathbf{B}(x)$] and takes no account of the intragrain circulating currents.

Figure 4 compares measured and calculated families of curves of the evolution of $\langle B_z\rangle_{\mathrm{wall}}$ vs μ_0H_ϕ. The growth of $\langle B_\phi\rangle_{\mathrm{wall}}$ vs H_ϕ is "traditional" and not shown. Here we simply note that, experimentally and theoretically, the entry and exit of azimuthal flux is facilitated by the presence of a static $H_\parallel$ [23]. For the theoretical curves, $j_{c\perp}=2.5(10^6)$ A/m^2, is taken independent of B (Bean approximation) in accord with the data of Fig. 3 and we let $j_{c\parallel}=j_{c\parallel}^*B_*/B$ (Kim-Anderson approximation). $B_*=B_p/2=\mu_0j_{c\perp}(R_0-R_i)/2=2.5$ mT and $j_{c\parallel}^*=j_{c\perp}$. Figure 5 compares the observed and calculated values for the max-

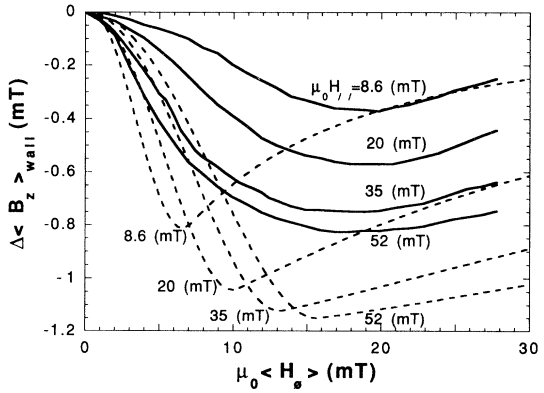

FIG. 4. Representative measured (solid) and calculated (dashed) curves of the evolution of $\langle B_z\rangle_{\mathrm{wall}}$ vs $\mu_0\langle H_\phi\rangle$. To provide a common baseline, the expulsion of axial flux from the wall during field cooling is not displayed.

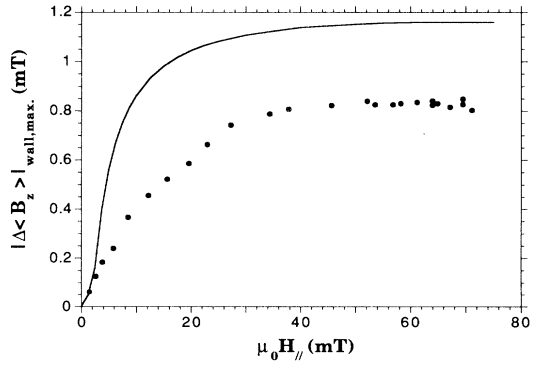

FIG. 5. The maximum expulsion of axial flux from the wall as $\langle H_\phi\rangle$ is impressed (see Fig. 4) is plotted vs the corresponding static $H_\parallel$. The data points are experimental; the solid curve is traced through the theoretical results.

imum excursion of $\langle B_z \rangle_{\text{wall}}$ as the valleys are traversed in various static $H_{\parallel}$.

It is noteworthy that the cutting and cross-flow of flux lines we encounter in the weak link regime of granular ceramics also occurs in the low range of H_{ϕ} in the monolithic and homogeneous classical materials studied by LeBlanc *et al.* [15].

We have demonstrated that the cutting and cross-flow of nonparallel flux lines occurs in the weak link regime of high-T_c superconductors. Our analysis gives estimates of the magnitude of $j_{c\parallel}$, the intergrain critical current density for flux line cutting and its dependence on B. Measurements of the rates of relaxation of $\langle B_z \rangle_{\text{wall}}$, $\langle B_{\phi} \rangle_{\text{wall}}$, $\langle B_z \rangle_{\text{hole}}$, and $\langle B_z \rangle_{\text{annular}}$ are in progress and yield information on the activation energy for thermally assisted flux line cutting and cross-flow.

[1] A. Sudbø and E. H. Brandt, Phys. Rev. Lett. **67**, 3176 (1991).

[2] E. H. Brandt and A. Sudbø, Phys. Rev. Lett. **66**, 2278 (1991).

[3] M. E. Cates, Phys. Rev. B **45**, 12415 (1992).

[4] S. P. Obukhov and M. Rubinstein, Phys. Rev. Lett. **66**, 2279 (1991); **65**, 1279 (1990).

[5] Ying-Hong Li and S. Teitel, Phys. Rev. Lett. **66**, 3301 (1991).

[6] H. Safar, E. Rodriguez, F. de la Cruz, P. L. Gammel, L. F. Schneemayer, and D. J. Bishop, Phys. Rev. B **46**, 14238 (1992).

[7] M. C. Marchetti and D. R. Nelson, Phys. Rev. B **41**, 1910 (1990).

[8] D. R. Nelson and M. S. Seung, Phys. Rev. B **39**, 9153 (1989); D. R. Nelson, Phys. Rev. Lett. **60**, 1973 (1988).

[9] B. D. Josephson, Phys. Rev. **152**, 211 (1966).

[10] M. G. Blamire and J. E. Evetts, Phys. Rev. B **33**, 5131 (1986); Appl. Phys. Lett. **46**, 1181 (1985).

[11] J. R. Cave and M. A. R. LeBlanc, J. Appl. Phys. **53**, 1631 (1982).

[12] G. Fillion, R. Gauthier, and M. A. R. LeBlanc, Phys. Rev. Lett. **43**, 86 (1979).

[13] J. R. Cave, J. E. Evetts, and A. M. Campbell, J. Phys. (Paris), Colloq. **39**, C6-614 (1978).

[14] D. G. Walmsley, J. Phys. F **2**, 510 (1972).

[15] M. A. R. LeBlanc, D. LeBlanc, A. Golebiowski, and G. Fillion, Phys. Rev. Lett. **66**, 3309 (1991).

[16] E. H. Brandt, Phys. Rev. B **25**, 5756 (1982); J. Low Temp. Phys. **44**, 33 (1981); **44**, 59 (1981); **39**, 41 (1980).

[17] E. H. Brandt, J. R. Clem, and D. G. Walmsley, J. Low Temp. Phys. **37**, 43 (1979).

[18] J. R. Clem, Phys. Rev. B **26**, 2463 (1982); Physica (Amsterdam) **107B**, 453 (1981); J. Low Temp. Phys. **38**, 353 (1980); Phys. Rev. Lett. **38**, 1425 (1977).

[19] J. R. Clem and A. Pérez-Gonzalez, Phys. Rev. B **33**, 1601 (1986); **30**, 5041 (1984).

[20] J. R. Clem and S. Yeh, J. Low Temp. Phys. **39**, 173 (1980).

[21] A. Perez-Gonzalez and J. R. Clem, Phys. Rev. B **43**, 7792 (1991); **42**, 4100 (1900); **32**, 2909 (1985); J. Appl. Phys. **58**, 4326 (1985).

[22] P. Wagenleithner, J. Low Temp. Phys. **48**, 25 (1982).

[23] G. Gandolfini, M. A. R. LeBlanc, and J. Sekerka, Cryogenics **29**, 373 (1989).